Sampling Jitter in Charge Sampling Radio

Ville Syrjälä, Vesa Lehtinen and Mikko Valkama

***Abstract*—This article addresses some implementation challenges in the potentially very energy-efficient charge-sampling radios. Alternative ways to implement charge sampler in charge sampling radio are considered, and the impacts and spectral shape characteristics of the sampling jitter induced signal distortion are analytically studied in these cases. The analysis shows that the spectrum of the distortion caused by the sampling jitter in a charge sampling receiver is not necessary flat, which in turn has direct impacts on the receiver design and dimensioning. The validity of the analytical results is verified with computer simulations. In simulations, both white Gaussian noise -type clock jitter and clock jitter generated by a phase-locked-loop oscillator are considered.**

***Index Terms*—Charge sampling; sampling jitter**

I. Introduction

CHARGE sampling, or charge-domain sampling, is a sampling technique that is based on integrating the signal current derived from the signal voltage, instead of sampling the signal voltage directly [1]. The approach potentially allows building energy-efficient sampling circuits that work at very high frequencies [1], [2], [3], [4]. In such circuits, sampling jitter still remains as one of the implementation problems.

Sampling jitter effects on charge sampled signal have been studied, e.g., in [5]. They derived a formula for signal-to-noise ratio (SNR) due to sampling jitter with assumption that the sampling jitter instants are mutually independent and uncorrelated white Gaussian noise. However, to our best knowledge, frequency domain behaviour of sampling jitter error in charge sampler (CS) has not been studied in existing literature. In this paper, we study the spectrum of the noise caused by the sampling jitter in CS. We show that the noise spectrum is not necessarily white, and in certain cases power spectrum has a strongly frequency-dependent shape. This is an important finding because the SNR is only deteriorated by noise within the band of interest, as out-of-band noise will be filtered out or at least attenuated.

The structure of the rest of the paper is as follows. In the second section, general charge sampling radio and general model for charge sampled bandpass-signal are derived. In the third section, the effect of the sampling jitter is analyzed in different charge-sampling receiver implementation cases. The analytical results and discussion in the third section are verified with simulations in the fourth section. In fifth section, charge-sampling receiver design-considerations are shortly given based on the spectral shape of the sampling-jitter error. Finally the sixth section concludes the work.

Notation in this paper is as follows. Sampling interval T_s is the time between the discrete samples at the sampler output and T_i is the integration time within the sampling interval during which the sample is integrated in the CS. Sampling rate is the inverse of the sampling interval.

The work was supported by TUT graduate school, Jenny and Antti Wihuri Foundation, HPY Research Foundation, Ulla Tuominen Foundation, the Academy of Finland, and the Finnish Funding Agency for Technology and Innovation.

The authors are with Department of Communications Engineering, Tampere University of Technology, P.O. Box 553, 33101 Tampere, Finland (email: {ville.syrjala, vesa.lehtinen, mikko.e.valkama}@tut.fi).

II. Charge Sampling Radio

This section gives general description of a charge sampling radio and a signal model for general IQ-modulated signal received by such radio.

A. General Description of Charge Sampling Radio

Charge sampling radios are proposed for direct RF sampling receiver architecture, e.g., in [2] and [3]. Principle structure of such direct RF sampling radio using charge sampling is illustrated in Fig. 1. In the structure, the signal is charge sampled after amplification and then processed further in sample domain. Unlike more traditional voltage sampler, CS does heavily shape the spectrum of the sampled signal. The frequency response of CS (magnitude response illustrated in Fig. 2 is $H(\omega) = c\,\mathrm{sinc}(T_i\omega/2)$, where ω is the angular frequency, T_i is the length of the integration interval used in CS, c is a constant that depends on the sampling circuit, and $\mathrm{sinc}(\cdot)$ is the unnormalized sinc function [1]. In order to tackle the signal corruption at the output of a CS, either 1) the incoming signal should be very narrowband with respect to the integration interval or 2) proper digital equalization should be done after the CS.

B. Model for Charge Sampled IQ-Signal

General operation of CS is illustrated in upper parts of Fig. 3 and Fig. 4. In model of Fig. 3, it is assumed that the previous integration interval always ends at the same time that the next integration interval begins. Fig. 4 on the other hand gives a more general CS model. In the more general model, integration window length is not necessary equal to the sampling interval. In Fig. 4, the same notation is used as in the following analysis.

Let us consider a general IQ-modulated continuous bandpass-signal

$$r(t) = x_I(t)\cos(\omega_c t) - x_Q(t)\sin(\omega_c t). \quad (1)$$

Here, ω_c is the carrier frequency, and $x_I(t)$ and $x_Q(t)$ are the I and Q components of the baseband message signal, respectively. When the bandpass signal is sampled with an ideal CS, (1) achieves the form

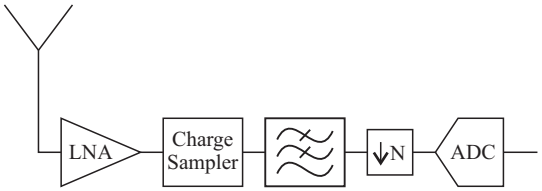

Fig. 1. Principal structure of charge sampling radio, consisting of low-noise amplifier, CS, lowpass filter, downsampler and analogue-to-digital converter.

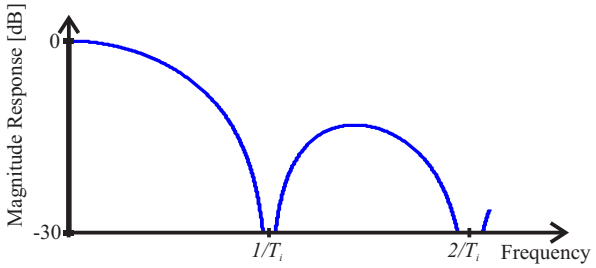

Fig. 2. Normalized (max. 0 dB) magnitude response of a charge sampler. T_i denotes the integration interval of the sampler.

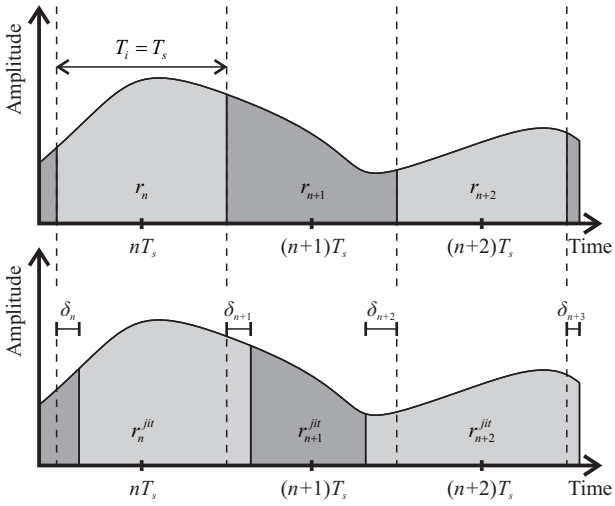

Fig. 3. An example demonstration of charge sampling in case 1. Here, next integration intervals starts when previous ends. Upper figure is without sampling jitter and lower figure is with sampling jitter. Dashed lines mark the ideal integration boundaries.

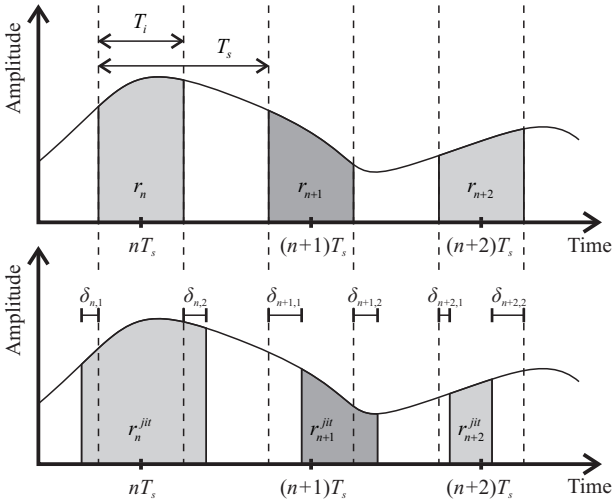

Fig. 4. A general demonstration of the charge sampling in case 2. There is a gap between the end of the previous and start of the next integration intervals. Upper figure is without sampling jitter and lower figure is with sampling jitter. Dashed lines mark the ideal integration boundaries.

$$r_n = \int_{nT_s - T_i/2}^{nT_s + T_i/2} \left[x_I(t)\cos(\omega_c t) - x_Q(t)\sin(\omega_c t) \right] dt = \int_{t - T_i/2}^{t + T_i/2} \left[x_I(\tilde{t})\cos(\omega_c \tilde{t}) - x_Q(\tilde{t})\sin(\omega_c \tilde{t}) \right] d\tilde{t} \Big|_{t = nT_s}, \quad (2)$$

where T_s is the sampling interval. From now on for the sake of compactness we mark $t_{n,1} = nT_s - T_i/2$ and $t_{n,2} = nT_s + T_i/2$. The samples correspond to those of the voltage sampler, but with the discussed filtering response. The response is also visible in (2), as the boxcar filtering in time domain corresponds to the sinc pulse in frequency domain.

III. Sampling Jitter in Charge Sampling Radio

Given a conventional voltage sampler, sampling jitter modelling is usually a simple task [6]. The clock signal that controls the sampler can simply be considered to be generated, e.g., by a phase-locked loop (PLL) oscillator or similar. The phase noise of such oscillator then gives directly a relatively good basis to model the statistics of the sampling jitter. However, modelling the jitter process in CS is not such a simple task. This section concentrates on the analysis, modelling and the effects of the sampling jitter in CS.

A. Charge Sampled Signal Corrupted by Sampling Jitter

Now, let us consider CS that is impaired by sampling jitter. The jitter only affects the integration intervals in (2), thus giving a signal model

$$r_n^{jit} = \int_{nT_s - T_i/2 + \delta_{n,1}}^{nT_s + T_i/2 + \delta_{n,2}} \left[x_I(t)\cos(\omega_c t) - x_Q(t)\sin(\omega_c t) \right] dt . \quad (3)$$

Here, $\delta_{n,1}$ and $\delta_{n,2}$ are the sampling jitters at the beginning and at the end of the nth integration period, respectively. Now, by using partial integration and denoting $t_{n,1}^{jit} = nT_s - T_i/2 + \delta_{n,1}$ and $t_{n,2}^{jit} = nT_s + T_i/2 + \delta_{n,2}$, we can separate (3) in two parts as

$$r_n^{jit} = \frac{1}{\omega_c}\left[x_I(t_{n,2}^{jit})\sin(\omega_c t_{n,2}^{jit}) + x_Q(t_{n,2}^{jit})\cos(\omega_c t_{n,2}^{jit}) - x_I(t_{n,1}^{jit})\sin(\omega_c t_{n,1}^{jit}) - x_Q(t_{n,1}^{jit})\cos(\omega_c t_{n,1}^{jit}) \right] - \frac{1}{\omega_c}\int_{t_{n,1}^{jit}}^{t_{n,2}^{jit}} \left[\frac{dx_I(t)}{dt}\sin(\omega_c t) + \frac{dx_Q(t)}{dt}\cos(\omega_c t) \right] dt . \quad (4)$$

Here, notation dy/dt refers to derivative of y with respect to t. Now, when using the partial integration again in the integral in (4), the result would once again be divided by ω_c. Because we consider direct RF sampling system, we are sampling relatively narrowband signal at a very high carrier frequency ω_c (around 10^{10} radians/s). From this it stems that when ω_c indeed divides the integral in (4), it makes the integral term diminishingly low-valued compared to the value of first term of (4). Thus we can approximate (4) as

$$r_n^{jit} \approx \frac{1}{\omega_c}\left[x_I(t_{n,2}^{jit})\sin(\omega_c t_{n,2}^{jit}) + x_Q(t_{n,2}^{jit})\cos(\omega_c t_{n,2}^{jit}) - x_I(t_{n,1}^{jit})\sin(\omega_c t_{n,1}^{jit}) - x_Q(t_{n,1}^{jit})\cos(\omega_c t_{n,1}^{jit}) \right]. \quad (5)$$

Now, since the I and Q components of the baseband signal are always multiplied with the corresponding high-frequency carrier components (sine and cosine waves), the time error caused by the sampling jitter to the I and Q components is very small compared to the time error caused to high-frequency carrier components [7]. We can thus further approximate (5) as

$$r_n^{jit} \approx \frac{1}{\omega_c}\Big[x_I(t_{n,2})\sin(\omega_c t_{n,2}^{jit}) + x_Q(t_{n,2})\cos(\omega_c t_{n,2}^{jit}) - x_I(t_{n,1})\sin(\omega_c t_{n,1}^{jit}) - x_Q(t_{n,1})\cos(\omega_c t_{n,1}^{jit})\Big]. \quad (6)$$

We also know that the jitter terms $\delta_{n,1}$ and $\delta_{n,2}$ in general are relatively small values, so we can use the well-known small phase approximation for the sine and cosine terms and get

$$\begin{aligned} r_n^{jit} \approx \frac{1}{\omega_c}\Big\{ & x_I(t_{n,2})\Big[\sin(\omega_c t_{n,2}) + \omega_c\delta_{n,2}\cos(\omega_c t_{n,2})\Big] \\ & + x_Q(t_{n,2})\Big[\cos(\omega_c t_{n,2}) - \omega_c\delta_{n,2}\sin(\omega_c t_{n,2})\Big] \\ & - x_I(t_{n,1})\Big[\sin(\omega_c t_{n,1}) + \omega_c\delta_{n,1}\cos(\omega_c t_{n,1})\Big] \\ & - x_Q(t_{n,1})\Big[\cos(\omega_c t_{n,1}) - \omega_c\delta_{n,1}\sin(\omega_c t_{n,1})\Big]\Big\}. \end{aligned} \quad (7)$$

This approximately gives the model for a signal sampled with CS impaired by the sampling jitter.

B. Sampling-Jitter Error in Charge Sampled Signal

Above we have derived a model for the sampling jitter impaired charge sampled signal in (7). With the same approximation used to obtain (5), the signal without sampling jitter can be written as

$$r_n \approx \frac{1}{\omega_c}\Big[x_I(t_{n,2})\sin(\omega_c t_{n,2}) + x_Q(t_{n,2})\cos(\omega_c t_{n,2}) - x_I(t_{n,1})\sin(\omega_c t_{n,1}) - x_Q(t_{n,1})\cos(\omega_c t_{n,1})\Big]. \quad (8)$$

It is thus trivial to derive the model for the actual error or distortion caused by the sampling jitter. As can be seen, (7) and (8) are already simplified to forms from which their difference is easily calculated. This difference is the error signal caused by the sampling jitter and can be written as

$$\begin{aligned} e_n^{jit} &= r_n^{jit} - r_n \\ &\approx \frac{1}{\omega_c}\Big\{\omega_c\delta_{n,2}\Big[x_I(t_{n,2})\cos(\omega_c t_{n,2}) - x_Q(t_{n,2})\sin(\omega_c t_{n,2})\Big] \\ &\quad - \omega_c\delta_{n,1}\Big[x_I(t_{n,1})\cos(\omega_c t_{n,1}) - x_Q(t_{n,1})\sin(\omega_c t_{n,1})\Big]\Big\} \\ &= \delta_{n,2}r(t_{n,2}) - \delta_{n,1}r(t_{n,1}). \end{aligned} \quad (9)$$

We can see that the noise caused by the sampling jitter is simply sum of two terms, $\delta_{n,2}r(t_{n,2})$ and $-\delta_{n,1}r(t_{n,1})$. Both of the terms are product of the sampling jitter and the IQ signal. The only difference between the two terms is timing. What the actual sampling jitter caused noise is like, especially in frequency domain, depends on the relationship between the sampling jitter and the IQ signal at the different moments in time ($t_{n,1}$ and $t_{n,2}$).

C. How to Model the Timing Jitter in Charge Sampler

The sampling jitter modelling depends on the hardware implementation of the sampler and the sampling clock. This is because in a CS the sampling jitter effect on a sample does not depend only on a time error caused by a simple timing offset in the time when the sample is taken. This is the case in voltage sampler, but in a CS, as Fig. 3, Fig. 4 and (9) illustrate, the error depends on the time error in the beginning and in the end of the integration period. One implementation approach assumes that timing jitter merely moves the boundary in which the previous integration ends and the next one starts. This assumption is made in the case in Fig. 3. In this case a sample window ends and the next window starts at the same instant, hence they share the same time offset. This corresponds to the case of jitter-free switches fed by a clock contaminated by jitter. A more general model is depicted in Fig. 4. There sampling jitter values $\delta_{n,1}$ and $\delta_{n,2}$ for $\forall n$ may either depend on each other, may not depend on each other, or only some of them may depend on each other, depending on the implementation of the CS. So the main question in sampling jitter modelling is how the sampling jitter terms in (9) depend on each other, and what kind of an effect does that have on the error caused by the sampling jitter.

D. Effect of the Sampling Jitter on Charge Sampler

Here sampling jitter effect is studied in two interesting cases.

1) Case 1

Case 1 is depicted in Fig. 3. In case 1 the next integration period start at the same time as the previous ends. This means that in (9) $\delta_{n,2} = \delta_{n+1,1} \triangleq \delta_{n+1}$ and $r(t_{n,2}) = r(t_{n+1,1}) \triangleq r(t_{n+1})$, as can be seen by comparing Fig. 3 and Fig. 4. Also, $r(t_n) = r(nT_s - T_s/2)$. Therefore, based on (9), the jitter can be written in the form

$$e_n^{jit} \approx \delta_{n+1}r(t_{n+1}) - \delta_n r(t_n). \quad (10)$$

This is equivalent to filtering signal $\delta_n r(t_n)$ with digital filter $H(z) = 1 - z^{-1}$. This means that the sampling jitter is directly the filtered product of the voltage sampled IQ-signal $r(t_n)$ and the sampling jitter process δ_n.

2) Case 2

The case 2 is the one depicted in Fig. 4. Here, $\delta_{n,1}$, $\delta_{n,2}$ and $\delta_{n+1,1}$ are not mutually pair-wise fixed to be equal to each other. The error term due to jitter is directly the one derived in (9), namely sum of terms $\delta_{n,2}r(t_{n,2})$ and $-\delta_{n,1}r(t_{n,1})$. If the sampling jitter process is assumed to be white Gaussian noise (WGN), then there is no filtering effect, and the resulting sampling-jitter noise is white. To show this explicitly, the correlation of the sampling-jitter-induced noise samples e_n^{jit} and e_k^{jit} for $k \neq n$ must be zero. From approximation in (9), we can conclude, that this is indeed the case in case 2 when sampling jitter process is assumed to be WGN. However, if all the sampling jitter terms $\delta_{n,1}$ and $\delta_{n,2}$ for $\forall n$ come from the same correlated process, e.g., the sampling jitter sequence is generated by PLL, there might be some filtering effect. This happens when $\delta_{n,2} \approx \delta_{n+1,1}$ and $r(t_{n,2}) \approx r(t_{n+1,1})$, namely when we are very close to the case 1, i.e. when T_i is near to T_s. In such case, the strength of the filtering effect depends on how close T_i actually is to T_s.

In case 2 it should be noted that if the integration interval length T_i is made narrower, also the charge integrated by the CS is relatively small. At the same time the power of the sampling-jitter noise, however, is not affected by the shorter integration period, resulting in relatively low SNR. Of course, not integrating all the time gives savings in used energy.

IV. Simulations and Simulation Analysis

In this section, we verify that simulations confirm the analytical results. This is verified by simple spectrum comparisons. In simulations a baseband equivalent OFDM signal with 12 MHz bandwidth is first created at sampling frequency 15.36 MHz. The signal is then 2^{18} times oversampled and IQ mixed around carrier frequency f_c of 867.5 MHz. These parameter values are selected for the sake of example. After the signal creation, the CS with jitter is modelled. We model a CS working at sampling frequency of 3932.16 MHz, so we are oversampling the baseband waveform by 2^8 times. This allows us to use the remaining 2^{10} times oversampling, to model the sampling jitter. Furthermore, we use linear interpolation to make the simulation of the sampling jitter even more accurate. The used PLL-type sampling-jitter sequence is generated with the PLL-type oscillator model used, e.g., in [8].

Simulation results are given in Figures 5 to 9. In these, term semianalytical refers to calculating sampling-jitter error using (9) and inputting the same waveforms to it as used in the simulations. The magnitude response of $H(z)=1-z^{-1}$ filter curve is also given in the figures where considered relevant.

Fig. 5 depicts the case 1 with 20-ps root-mean-square (RMS) WGN-type sampling jitter. As expected, the simulations confirm the analytical results. The sampling jitter caused error indeed has the shape of $H(z)=1-z^{-1}$ discrete time filter. In case of PLL-type sampling jitter in Fig. 6, we can see the same shaping effect. In Fig. 7, the case with PLL-type sampling jitter for which $\delta_{n,1}$ and $\delta_{n,2}$ come from the separate PLLs is depicted (this corresponds to case 2 with $T_i = T_s$). When comparing the results of Fig. 6 to results of Fig. 7, we can indeed see that the former results have the clear filtering effects present, whereas the latter results do not have any filtering effect at all. In Fig. 7, we only see the resulting spectrum when the information signal is multiplied with the sampling jitter sequence.

Now, for the case 2 results change a little. For WGN-type sampling jitter, there is no noise shaping at all. The sampling jitter caused noise is thus WGN as well. Fig. 8 and Fig. 9 depict the case with PLL-type noise in case when sampling jitter is generated with a single PLL, for $2T_i = T_s$ and $4T_i = T_s$, respectively. In this case, $\delta_{n,1}$ and $\delta_{n,2}$ correlate with each other. We can see that, as expected, in $2T_i = T_s$ case there is still minor filtering effect visible, but as integration interval gets narrower and narrower (e.g. $4T_i = T_s$), the filtering effect ceases to exist due to lack of correlation either between $\delta_{n,2}$ and $\delta_{n+1,1}$ or between $r(t_{n,2})$ and $r(t_{n+1,1})$.

V. Impact on Receiver Design

The spectral shape of the sampling jitter in the sampling clock signal that controls a CS has been ignored in most of the earlier studies in the literature. Such is the case, e.g., in our case 2 with the white Gaussian noise like jitter model, when the sampling jitter at the end of the previous integration period and at the beginning the current integration period are not dependent on each other. However, when CS is implemented so that the sampling jitter at the end of the previous integration period equals to, or is heavily depends on, the sampling jitter at the beginning of the next integration period, the error caused by the sampling jitter is not white anymore. This must be taken into account in the receiver design as is demonstrated in Fig. 10.

Fig. 10 demonstrates the signal and the jitter-noise shaping in case 1 when WGN shaped sampling jitter is assumed. The figure tells how the signal or sampling-jitter noise is shaped

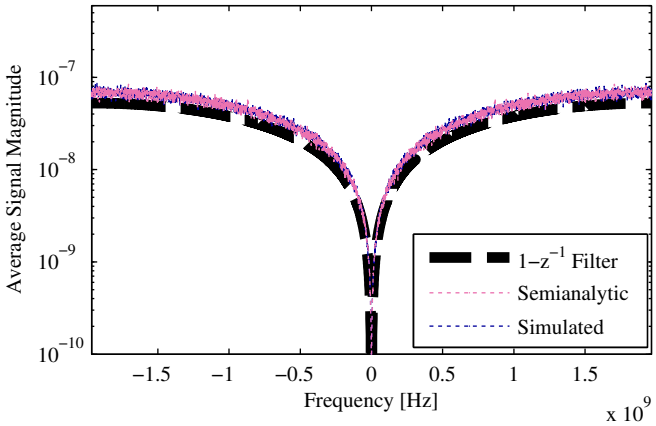

Fig. 5. Error spectrum caused by sampling jitter, when jitter is white Gaussian noise. 20-ps RMS jitter, case 1 (with $T_i = T_s$).

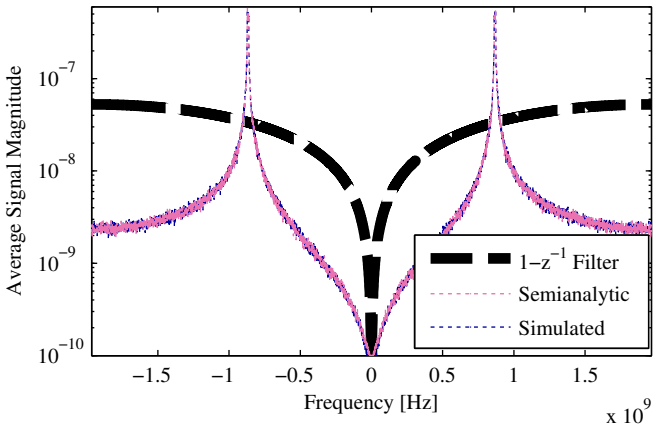

Fig. 6. Error spectrum caused by sampling jitter when jitter is generated by PLL oscillator. 20-ps RMS jitter, case 1 (with $T_i = T_s$).

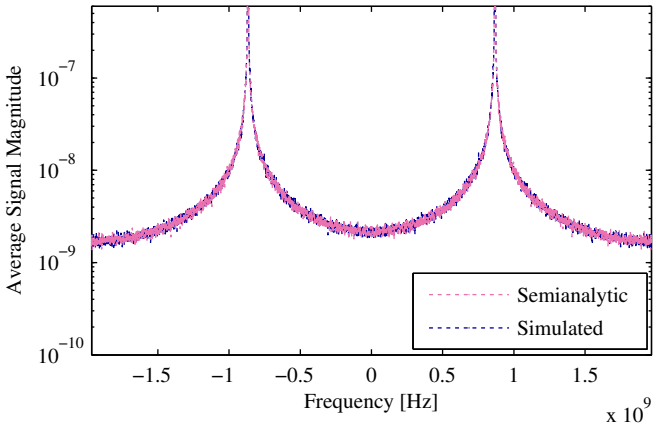

Fig. 7. Error spectrum caused by sampling jitter when jitter is generated by PLL oscillator, but sampling jitters at the beginnings and the ends of the integration intervals are independent of each other. 20-ps RMS jitter, case 2 (with $T_i = T_s$).

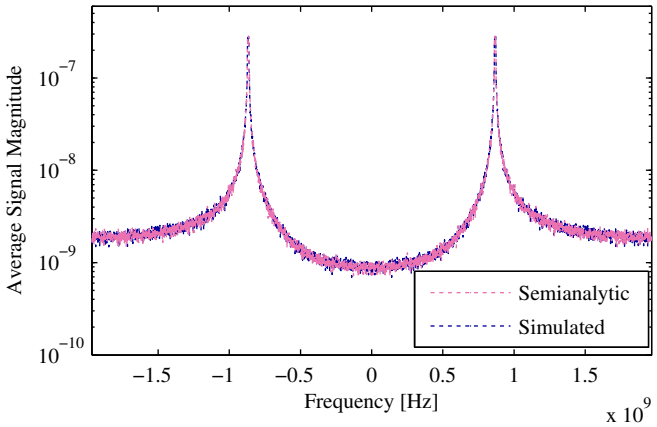

Fig. 8. Error spectrum caused by sampling jitter when jitter is generated by PLL oscillator. 20-ps RMS jitter, case 2 (with $2T_i = T_s$).

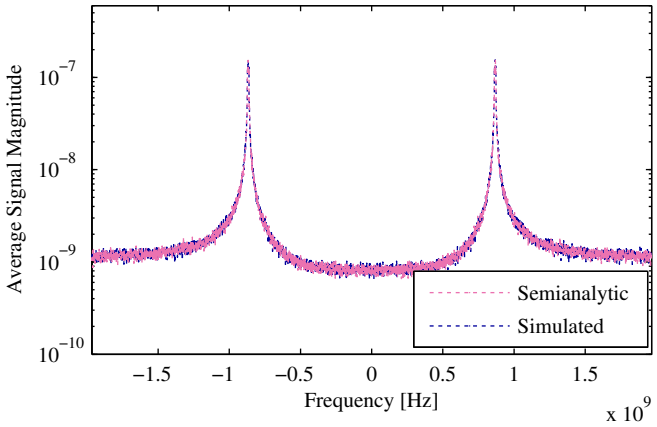

Fig. 9. Error spectrum caused by sampling jitter when jitter is generated by PLL oscillator. 20-ps RMS jitter, case 2 (with $4T_i = T_s$).

when the useful signal is at a certain carrier (or centre) frequency (horizontal axis). Signal response curve gives the basic signal response without sampling jitter, jitter noise response curve is the response that was derived for the sampling jitter in this work, signal-to-jitter-noise density gain curve is the gain in signal-to-jitter-noise ratio compared to traditional voltage sampling scheme, and finally signal-to-noise density ratio curve has also the additive thermal noise in addition to sampling jitter.

In case 1, the receiver designer can exploit the sampling jitter spectrum by adjusting the relationship between carrier frequency f_c and sampling rate F_s so that the information signal is in a region where sampling jitter is attenuated and the useful signal is not. This only happens when very high oversampling is used as Fig. 10 suggests. The same can be done for case 2 when the filtering effect is present, namely in case when the sampling jitter is generated with a single PLL process and when T_i and T_s are relatively close to each other. In other cases, the spectrum of the sampling jitter behaves similarly as in the voltage sampling.

For example, in [9] bandpass CS is used to sample a radio signal with centre frequency f_c at sampling rate $F_s = 2f_c$. Unfortunately, Fig. 10 shows that the jitter noise shaping observed in case 1 boosts the jitter noise at these frequencies. On the other hand, the jitter-noise notches coincide with the signal notches, the only exception being the jitter-noise notch at the zero frequency, where the advantages can be achieved, with a cost of high sampling frequencies of course.

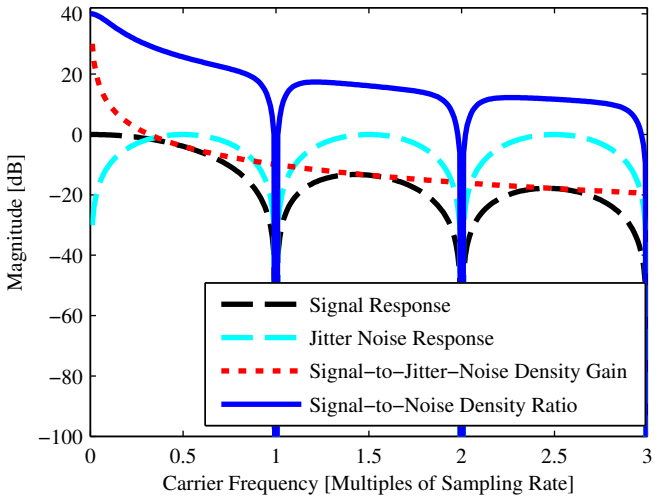

Fig. 10. Signal and noise shaping of case 1 CS. Horizontal axis is the carrier (or centre) frequency of the relatively narrowband signal waveform. For the signal-to-noise density ratio curve, 40-dB SNR due to thermal noise is assumed. Unshaped jitter noise power is 30 dB under the signal power.

VI. Conclusion

As in all systems that sample high-frequency signals, sampling jitter is also an interesting phenomenon in charge sampling radio. We studied the spectral shape of the sampling-jitter induced noise in various charge sampler implementation scenarios. In certain implementations, the charge sampler shapes the spectrum of sampling jitter generated noise in a way that differs from the way the spectrum of the useful signal is shaped. This difference can and should be exploited directly in receiver design, to optimize the receiver chain SNR.

References

[1] L. R. Carley and T. Mukherjee, "High-speed low-power integrating CMOS sample-and-hold amplifier architecture," in *Proc. Custom Integrated Circuits Conference*, Santa Clara, CA, May 1995, pp. 543-546.

[2] J. Yuan, "A charge sampling mixer with embedded filter function for wireless applications," in *Proc. International Conference on Microwave and Millimeter Wave Technology*, Beijing, China, September 2000, pp. 315-318.

[3] K. Muhammad *et al.*, "A discrete-time Bluetooth receiver in a 0.13µm digital CMOS process," in *Proc. International Solid-State Circuits Conference*, San Francisco, CA, February 2004.

[4] R. Bagheri *et al.*, "Software-defined radio receiver: dream to reality," IEEE Communications Magazine, Vol. 44, No. 8, pp. 111-118, August 2006.

[5] S. Karvonen, Thomas Riley, and J. Kostamovaara, "On the effects of timing jitter in charge sampling," in *Proc. Internation Symposium on Circuits and Systems*, Bangkok, Thailand, May 2003, pp. I-737-740.

[6] M. Shinagawa, Y. Akazawa, and T. Wakimoto, "Jitter analysis of high-speed sampling systems," *IEEE Journal of Solid-State Circuits*, Vol. 25, No. 1, pp. 220-224, February 1990.

[7] V. Syrjälä, M. Valkama, and M. Renfors, "Design considerations for direct RF sampling receiver in GNSS environment," in *Proc. Finnish Wireless Comm. Workshop*, Oulu, Finland, August 2007, pp. 9-13.

[8] N. N. Tchamov, V. Syrjälä, J. Rinne, M. Valkama, Y. Zou, and M. Renfors, "System- and circuit-level optimization of PLL designs for DVB-T/H receivers", *Analog Integrated Circuits and Signal Processing Journal*, January 2012, 10.1007/s10470-011-9823-2.

[9] Y-C Ho *et al.*, "Charge-domain signal processing of direct RF sampling mixer with discrete-time filter in Bluetooth and GSM receivers," *EURASIP Journal on Wireless Communications and Networking*, Vol. 2006, pp. 1-14, March 2006.